published in: Acta Materialia 57, 2009, 2376-2389

The thermodynamics of and strengthening due to co-clusters: general theory and application to the case of Al-Cu-Mg alloys

M.J. Starink and S.C. Wang

Materials Research Group, School of Engineering Sciences,
University of Southampton, Southampton S017 1BJ, UK

submitted 13 Aug 2008; accepted 19 Jan 2009

Abstract

Co-clusters in ternary or higher order metallic alloys are metastable structures involving two or more distinct alloying atoms that retain the structure of the host lattice. A thermodynamic model based on a single interaction energy of dissimilar nearest neighbour interaction energy is presented, and a model for the strengthening due to these co-cluster dimers is derived. The model includes a new treatment of (short-) order strengthening relevant to these co-clusters and further encompasses modulus hardening and chemical hardening. The models are tested against data on a wide range of Al-Cu-Mg alloys treated at temperatures between 20 and 220ºC. Both quantitative calorimetry data on the enthalpy change due to co-cluster formation and strengthening due to co-clusters is predicted well. It is shown that in general (short-range) order strengthening will be the main strengthening mechanism.

Keywords: Ageing; nanostructure; modelling; thermodynamics; short range ordering

Introduction

Clusters, co-clusters and their strengthening in metallic alloys

The prevailing theory of strengthening of metallic alloys as developed since the 1930s recognises the contributions to the critical resolved shear stress of grains with dilute compositions as being due to the obstacles to dislocation motion in the form of solute atoms and stable or metastable second phases. These second phases often form in a precipitation process from a supersaturated solution, and several metastable structures can appear before ultimately the stable phase or phases are formed. These precipitates can be very small: precipitates as small as 10 atoms have been proposed. These small precipitates are effectively formed from a metastable solution through a solute clustering process, i.e. the clustered solute atoms are situated on position of the host lattice. If the clusters formed involve two alloying elements, the term co-clusters is employed; the simplest form of a co-cluster is a dimer (Fig. 1). In most microstructural investigation techniques, including transmission electron microscopy (TEM) and high resolution electron microscopy (HREM) clusters of this small size can not be resolved. But atom probe experiments do allow detection of the clusters, and in the past two decades, 3D atom probe has allowed the identification of clusters as small as 10 atoms in alloys such as in maraging Fe-20Ni-1.8Mn-1.5Ti-0.59Al steel [1], Fe-C–Mn–Si steels with additions of Nb, Al and Mo [2], Al-Zn-Mg(-Cu) [3,4], Al-Mg-Ag [5], Al-Si-Mg [6]

and Al-Cu-Mg based alloys [7] (in the aluminium alloys the term Guinier-Preston (GP) zone has been associated with these clusters). The picture starting to emerge from two decades of atom probe work is that whenever the early stages of decomposition of solution treated alloys with significant alloying additions (significant in terms of influencing mechanical properties) are investigated, clusters or co-clusters are in most cases detected.

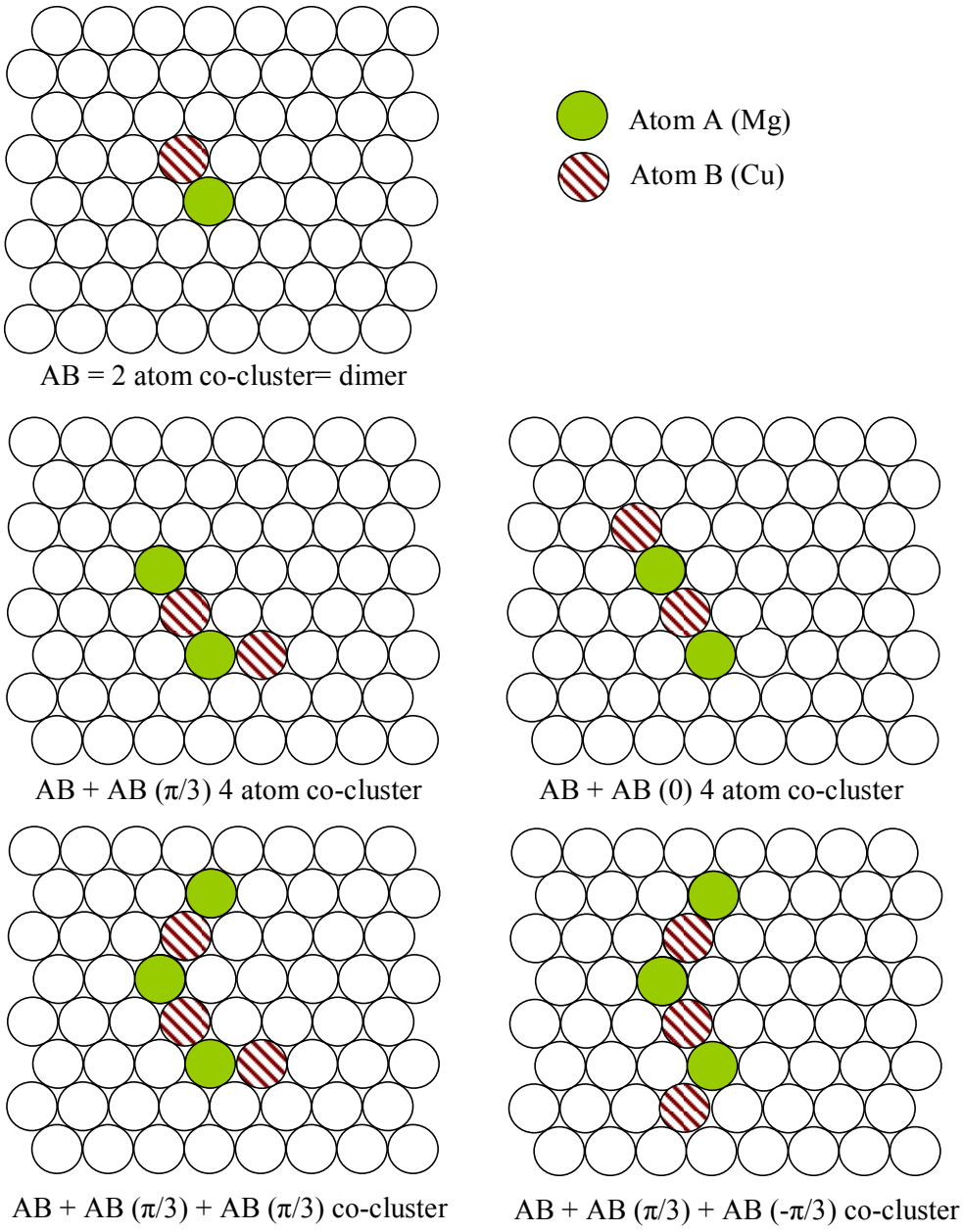

Fig. 1 A 111 plane in an FCC lattice in a ternary alloy containing co-clusters, with a notation describing the co-cluster constellation.

Hardening due to the clusters and co-clusters has been invoked as a qualitative explanation for strengthening of a range of alloys. However, attempts at providing a quantitative explanation of the strengthening effect of clusters and co-clusters have been limited and have been based on a limited physical basis. In this paper we will present a theory for the thermodynamics of and the

strengthening due to co-clusters in metallic alloys; thus providing the theoretical basis for this strengthening mode in metallic alloys. The model is applied to Al-Cu-Mg alloys and tested against an extensive amount of published and new data. This alloy system is chosen for the interlinked reasons of alloy availability, data availability, relative ease of sample preparation and analysis, and importance in engineering applications. Al-Cu-Mg alloys are extensively used for lightweight, fatigue resistant structures such as lower wing skins and fuselage of airplanes [8,9] as well as a range of other applications. The general validity of the theory is thought to not be limited to the investigated alloys: the developed theory will indicate that co-cluster formation should occur in many supersaturated alloys.

The method of choice for identifying thermodynamics of the co-clusters is calorimetry, as through calorimetry both the enthalpy changes of the system and the metastable solvi can be determined. However, calorimetry, in isolation, can not identify clusters or phases. Indications for the existence of co-clusters have mostly been obtained with 3 dimensional atom probe (3DAP) (and more recently supported by Nuclear Magnetic Resonance (NMR) [10,11], X-ray absorption spectroscopy (XAS) [12] and positron annihilation lifetime spectroscopy (PALS) studies [13]).

Co-clusters in Al-Cu-Mg alloys

For solution treated Al-Cu-Mg based alloys with composition in the α+S phase field, room temperature hardening occurs within several days (several weeks if the Cu content is very low) and hardening during artificial ageing is very fast, typically within minutes [14,15,16]. Whilst diverging explanations have been proposed for this phenomenon, recent experiments in combination with careful reassessment of existing evidence has indicated that the phenomenon is caused by Cu-Mg co-clusters [7]. In assessing the experimental evidence, we should note that immediately after the rapid hardening and during the room temperature hardening in these Al-Cu-Mg based alloys no distinct precipitate phase can be detected by conventional TEM [17], but differential scanning calorimetry (DSC) experiments clearly show a change in the free energy of the alloys indicating that a significant fraction of the dissolved atoms have been involved in a reaction [18,19]. There are no reports of any ordered structures at this stage. Results from several atom probe field ion microscopy (APFIM) and three-dimensional atom probe (3DAP) studies reveal Cu-Mg co-clusters of typically 1 nm diameter (10-40 atoms) [7,20,21] which by some authors are held directly responsible for the rapid hardening reaction [20,21]. Information on the composition of Cu-Mg co-clusters is limited. Ringer et al. [20,21] observed that in a high purity Al-1.7at.%Mg-1.1at.%Cu aged for 5 min at 150ºC clusters with high Cu:Mg ratios existed, whilst Starink et al. [7] found that in an Al-2.78wt%Cu-0.44wt%Mg and in an Al-2.78wt%Cu-1.05wt%Mg (both alloys are commercial purity with Mn additions) the Mg/Cu ratio of the clusters varied from one cluster to another. They also contain vacancies [17].

Due to the discovery of rapid hardening Al-Cu-Mg based alloys early in the 20th century, and its subsequent extensive application, the reaction has been extensively studied and it can be considered one of the classic issues in metallurgy. But early researchers did not have the benefit of HREM and atom probe analysis, and some unsubstantiated assumptions have entered the literature. Especially

in pre-1990s work early hardening reaction in Al-Cu-Mg alloys was attributed to the formation of Cu and Mg containing structures which were termed Guinier-Preston-Bagaryatski (GPB) zones [22]. This term was coined in the 1950s and has been used for decades without evidence of what they may consist of. Consequently a range of often conflicting interpretations of these GPB zones have appeared in the literature. Only very recently a clearer picture of GPB zones using scanning transmission electron microscopy (STEM) supported by first principle modelling of the structures is starting to emerge [23]. It is the opinion of the authors that due to differing interpretation of its meaning and the lack of experimental evidence, the term 'GPB zone', as related to the rapid hardening in Al-Cu-Mg based alloys, has become an obstacle to the proper understanding of the mechanisms for rapid hardening. Hence we will here avoid using the term as much as possible.

A model for the thermodynamics of and strengthening due to co-clusters

The thermodynamics of co-clusters

For modelling the thermodynamics of the co-clusters one may consider the possibility of the co-clusters forming a range of possible constellations in the FCC lattice. From a virtually unlimited number of possible constellations, some possible constellations that are thought to be energetically favoured in Al-Cu-Mg alloys (see Discussion section) are illustrated in Fig. 1. The smallest co-cluster is a dimer of nearest neighbours of dissimilar alloying atoms Fig. 1a. In considering an approach to modelling the thermodynamics, we considered three approaches to modelling in order of increasing complexity:

I. a regular solution model
II. a quasi-chemical model which takes nearest neighbour interactions into account (see e.g. [24]).
III. a first principles total energy calculation (FP-CVM) (see for instance [25]).

As described below, a dimer treated in a regular solution model (with a single bond energy), was found to fully explain all of a very extensive set of calorimetry data on Al-Cu-Mg alloys. Hence we will fully describe this treatment, and limit our consideration of more complex treatments to a brief discussion at the end of this subsection.

Within the regular solution model, the solvi of the phases and co-clusters in the ternary system can be derived as follows. Consider alloying elements A and B in a host metal M, the total number of the respective elements in the system are N_A, N_B and N_M. The Gibbs free energy, G, of the system can be approximated as:

$$G = H_o - N_{cl}\Delta H_{A-B} - TS \qquad (1)$$

where N_{cl} is the number of A-B dimers, H_o is a constant reference enthalpy and $\Delta H_{A\text{-}B}$ is the enthalpy of formation of an A-B dimer from the random solution, i.e. the enthalpy of the reaction in which one A atom and one B atom, originally in random solution, form an A-B dimer. The entropy of the system is proportional to the logarithm of the number of states w in the system:

$$S = k_B \ln w = k_B \ln\left(\frac{N!}{\left(N_M!\left(N_A - N_{cl}\right)!\left(N_B - N_{cl}\right)!12N_{cl}!\right.}\right) \tag{2}$$

where k_B is Boltzmann's constant. For equilibrium it holds $\partial G/\partial N_{cl}=0$. Performing this derivation using the latter two equations (using the Stirling approximation $\ln N!=N\ln N-N$) then provides that at equilibrium:

$$c_A c_B = \exp(-2)\exp\left[\frac{-\Delta H_{A-B}}{RT}\right] \tag{3}$$

where c_A is the solubility (i.e. the equilibrium molar fraction) of element A in the M rich host lattice, c_B is the solubility of element B in the M rich host lattice. It can be noted that this corresponds to the more generally applied 'solubility product' equation:

$$c_A c_B = C^2 \exp\left[\frac{-\Delta H_{A-B}}{RT}\right] \tag{4}$$

where C is a constant. In the latter form, no attempt is made to fully analyse the entropy term, and only the entropy of the atoms belonging to the Al-rich phase is considered. Thus constant C, which is related, amongst others, to the entropy of the clusters or precipitates, is considered a fittable parameter. In a more general form, the solubility limits of co-clusters according to the regular solution of any complex $M_mA_aB_b$ is given as:

$$c_A{}^a c_B{}^b = C^2 \exp\left[\frac{-\Delta H_{MmAaBb}}{RT}\right] \tag{5}$$

where ΔH_{MmAaBb} is the enthalpy of formation of the $M_mA_aB_b$ complex, i.e. the enthalpy of the reaction in which a atoms of type A, b atoms of type B and m atoms of type M, originally part of the M rich phase, form an $M_mA_aB_b$ complex, which can be an ordered or disordered cluster or precipitate.

The latter two expressions can be tested through measurement of the heat evolved in the reactions of formation or dissolution of the clusters or precipitates. Particularly, when a calorimetry experiment is conducted such that the total heat evolved on completing of the co-clustering reaction is measured, exothermic heat evolved, ΔQ, should then be given by:

$$\Delta Q = \frac{\left(x_A^o - x_A\right)}{a}\Delta H_{MmAaBb} \tag{6}$$

where x_A^o is the composition of the M-rich phase at the start of the reaction, and x_A is the composition of the M-rich phase on completion of the reaction. x_A can be solved by considering that the composition during the reaction up to completion of the reaction is given by:

$$x_A^o - x_A = \frac{a}{b}\left(x_B^o - x_B\right) \tag{7}$$

whilst at completion:

$$c_A^{\,a} c_B^{\,b} = x_A^{\,a} x_B^{\,b} \quad \text{(at completion of reaction)} \tag{8}$$

Thus x_A can be solved from Eqs. 5, 7 and 8. (For particular values of the ratio *a:b*, the equations can be solved analytically, particularly $a=b=1$ simplifies the equations considerably, but in general a simple iterative scheme is needed.)

An alternative treatment suggested in the literature [24] involves a quasi-chemical model which takes nearest neighbour interactions into account. Analysis of this model (see Discussion section) showed that it can not explain all the experimental observations.

Solution treated commercial alloys typically contain some small amounts of undissolved intermetallic phases or dispersoids, which reduce the amount of solute atoms available for co-cluster formation and subsequent precipitation. The composition of the supersaturated f.c.c. phase after solution treatment can generally be predicted from thermodynamic models (e.g. phase diagrams of the alloy). In commercial and commercial purity Al-Cu-Mg based alloys, ω-Al_7Cu_2Fe, S-Al_2CuMg and T-$Al_{20}Cu_2Mn_3$ can be present [26,27]. A method for calculating the amounts of these phases is described in the Appendix. This method is applied for all model predictions.

Strengthening due to co-clusters

Clusters and co-clusters are shearable and hence the Orowan strengthening mechanism is not applicable. Several strengthening mechanisms related to obstacle shearing need to be considered:

a) Order strengthening (including stacking fault strengthening) or configurational strengthening
b) Modulus hardening
c) Chemical hardening

Order strengthening

The strengthening due to an ordered phase which contains short or long range order depends on the way the dislocations interact with the precipitate or clusters. If long range order is present, dislocations can travel in groups due to the anti phase boundary (APB) [28,29,30,31,32]. For the present case of co-cluster strengthening, the order can be considered to be extremely short ranged and as restoration of order by dislocations travelling in groups is not possible, dislocations will travel alone. The work done in deforming the lattice through movement of dislocations hampered by (co-)clusters equals the change in energy related to the short range order per unit area on slip planes, i.e. [33,34]:

$$\Delta\tau_{sro} = \frac{\gamma_{sro}}{b} \tag{9}$$

where γ_{sro} is the change in energy per unit area on slip planes (which in most cases are {111} planes) on the passing of one dislocation (a.k.a. the diffuse interphase boundary energy [33,35]). In the analysis of γ_{sro} we could attempt to include several orders of near neighbour interaction for

instance through considering a cluster variation approach [36]. However, we will here use a simplified approach that considers only nearest neighbour interactions. This is done for the following reasons: i) we do not have sufficient accurate data to determine all the k^{th} interaction parameters, and ii) the simpler nearest neighbour method provides a more intuitively acceptable analysis, which is a benefit as several competing analysis of strengthening due to co-clusters have been accepted. We will consider here co-clusters that consist of a single pair of atoms A and B. The amount of A atoms in the co-clusters is y_A, the amount of B atoms in the co-clusters is y_B. The amount of A atoms in the M-rich phase is x_A, the amount of B atoms in the M-rich phase is x_B. In the (M-rich) f.c.c. lattice structure each atom has 12 nearest neighbours and each atom adjacent to a slip plane will have 3 nearest neighbours on the other side of the {111} slip plane. The area density of A-B nearest neighbour bonds crossing the slip plane is:

$$\rho_{A-B}(n_d = 0) = \frac{(y_A + y_B)}{S_{111}} = \frac{4(y_A + y_B)}{\sqrt{3}b^2} \tag{10}$$

where S_{111} is the area on the 111 plane occupied by one atom. On passing of one dislocation through the AB co-cluster a part of the A-B bonds present before the passing will be destroyed and some will be retained (see Fig. 2).

From the geometry of the f.c.c. lattice it follows that for a single dislocation on the 111 plane, 1/3 of the A-B nearest neighbour pairs will remain nearest neighbours. The passing through of a dislocation can also create A-B nearest neighbour pairs. The area density is given by $2/3y_Ax_B + x_Ax_B + 2/3y_Bx_A + x_Ax_B = 2/3y_Ax_B + 2/3y_Bx_A + 2x_Ax_B$. Thus the total area density of A-B nearest neighbour bonds crossing the slip plane after passage of one dislocation is:

$$\rho_{A-B}(n_d = 1) = \frac{4}{\sqrt{3}b^2}\left[\frac{1}{3}(y_A + y_B) + \frac{2}{3}y_Ax_B + \frac{2}{3}y_Bx_A + 2x_Ax_B\right] \tag{11}$$

The change in area density of A-B nearest neighbour bonds crossing the slip plane on passing of one dislocation is

$$\rho_{A-B}(n_d = 0) - \rho_{A-B}(n_d = 1) = \frac{4}{\sqrt{3}b^2}\left[\frac{2}{3}(y_A + y_B) - \left(\frac{2}{3}y_Ax_B + \frac{2}{3}y_Bx_A + 2x_Ax_B\right)\right]$$
$$\cong \frac{4}{\sqrt{3}b^2}\frac{2}{3}(y_A + y_B) \tag{12}$$

where the approximation is valid for dilute alloys. Passage of further dislocations will cause further changes in area density of A-B nearest neighbour bonds crossing the slip plane. As the magnitude of these changes will decrease on passing of each further dislocation, the first dislocation experiences the greatest resistance. Considering in approximation that the energy related to co-clusters is defined by the enthalpy of the nearest neighbour bond $\Delta H_{A\text{-}B}$ we can approximate:

$$\Delta\tau_{sro} = \frac{\gamma_{sro}}{b} = \frac{\Delta H_{A\text{-}B}}{b}\left[\rho_{A-B}(n_d = 0) - \rho_{A-B}(n_d = 1)\right]$$
$$= \frac{\Delta H_{A\text{-}B}}{b^3}\frac{4}{\sqrt{3}}\left[\frac{2}{3}(y_A + y_B) - \left(\frac{2}{3}y_A x_B + \frac{2}{3}y_B x_A + 2x_A x_B\right)\right] \quad (13)$$

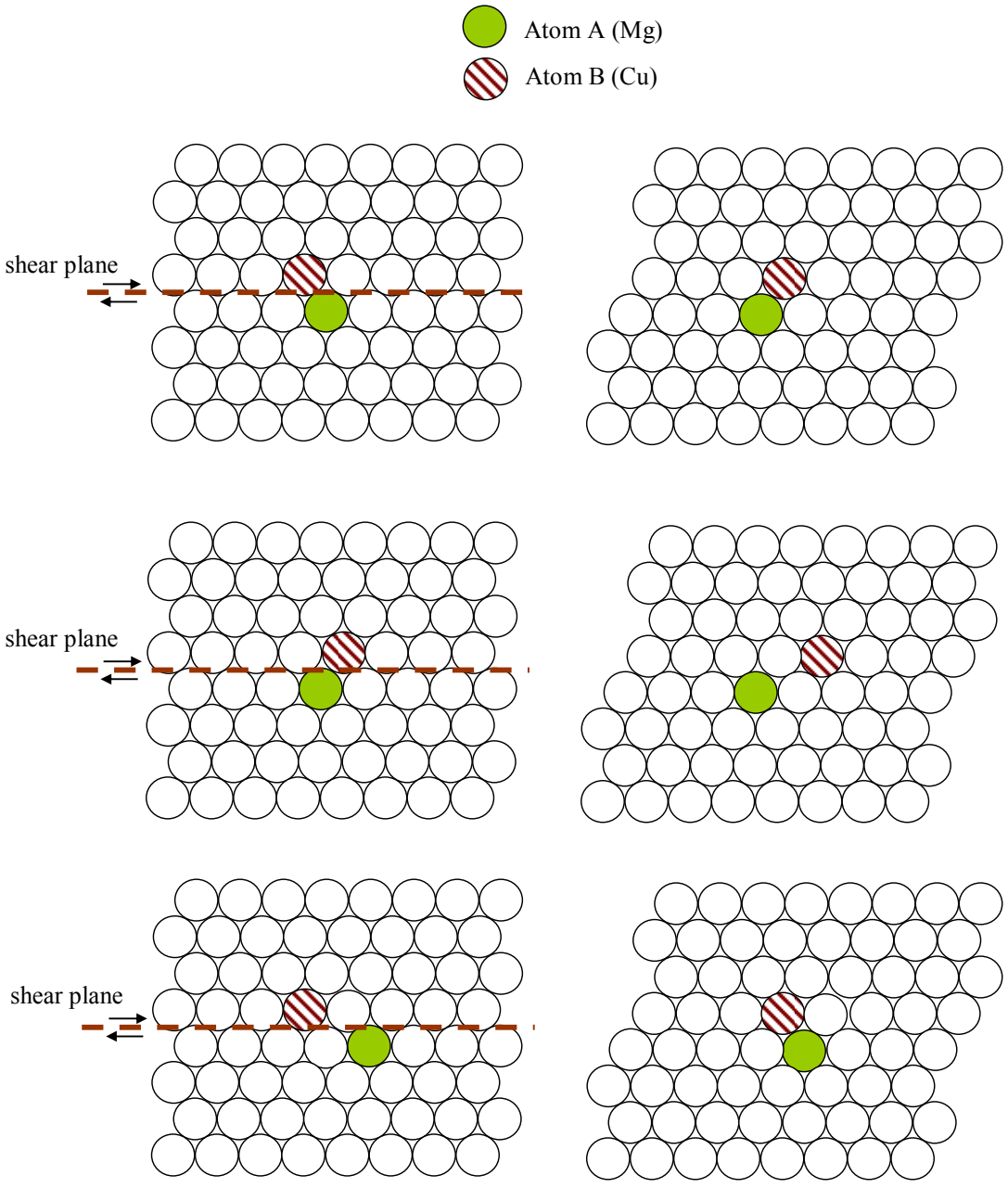

Fig. 2 A 111 plane in an FCC lattice with a 2 atom co-cluster being cut by a dislocation. Top shows before and after with the co-cluster remaining intact in a rotated form; middle shows before and after with the co-cluster being eliminated, which requires an energy input; and bottom shows before and after in the case where the passing of one dislocation creates a co-cluster, which releases energy.

Modulus hardening

Modulus hardening is a strengthening mechanism that is difficult to deal with theoretically [28], leading to quite complex expressions. The very much simplified treatment by Cartaud et al [37] (see also Ref. [38]), which has been adopted in a range of works, approximates the strengthening due to difference in shear modulus as:

$$\Delta\tau_{\mathrm{m}} = \frac{\Delta\mu}{4\pi\sqrt{2}}\sqrt{f^{\mathrm{cl}}} \tag{14}$$

where f^{cl} is the volume fraction of the clusters and $\Delta\mu$ is the difference in shear modulus between zones, μ_{cl}, and surrounding metallic phase. In the works that apply the latter equation, μ_{cl} has invariably been determined by fitting to strength data. A more realistic way of obtaining μ_{cl} is by approximating it as a weighted average of the moduli of the individual pure substances, i.e. for an $M_mA_aB_b$ cluster:

$$\mu_{cl} = \frac{m\mu_M + a\mu_A + b\mu_B}{m + a + b} \tag{15}$$

For example, for larger clusters in Al-Cu-Mg, where Cu, Mg and Al content may be tending towards the composition of S (i.e. 25%Cu, 25%Mg and 50%Al) the above equation gives an estimation of $\mu_{cl,}$ of 30GPa (using μ_{Al} = 26.2GPa, μ_{Cu} = 48.3GPa and μ_{Mg} = 17.3GPa from [39]).

A more detailed approximation of the modulus hardening can be obtained by a calculation of the interaction forces of screw and edge dislocations (including the maximum interaction force F_o) as they pass through the area (precipitate) with differing modulus. This type of calculation has been performed by Nembach [40] for a spherical precipitate and various models of the dislocation. Based on Friedel's approximation:

$$\Delta\tau = 1.4\frac{F_o^{3/2} f^{1/2}}{rb(2\pi S)^{1/2}} \tag{16}$$

Nembach's analysis [40] showed that the critical shear stress due to modulus hardening can be represented as:

$$\Delta\tau_m = 1.4\alpha^{3/2}\Delta\mu^{3/2} f^{1/2} b\left(\frac{r_p}{b}\right)^{3\beta/2-1}(2\pi S)^{-1/2} \tag{17}$$

where S is the dislocation line tension, and α and β are parameters that are obtained from the dislocation precipitate interaction models. As different dislocation core models predict somewhat different interaction forces between dislocation and precipitate, some uncertainty in $\Delta\tau_{\mathrm{m}}$ results. Averaged values are obtained for α = 0.096 and β = 0.76, respectively.

Chemical hardening

Chemical hardening, in its classical meaning, is due to the interfacial energy between precipitate and matrix, and strength increments a linearly proportional to this interfacial energy. It is

conceptually difficult to relate a cluster (even a dimer) to an interfacial energy. As an estimate of $\Delta\tau_{ch}$ we considered the classical expression for chemical hardening and the value for the interfacial energy provided in [7]. This predicts $\Delta\tau_{ch} \sim 0.03\ \Delta\tau_{sro}$, i.e. $\Delta\tau_{ch}$ is virtually negligible.

Experimental

The compositions of the alloys studied are presented in Table 1. Alloy 1 was produced as sheet through casting, homogenising, hot rolling in several passes, solution treatment at 500ºC and subsequent cold deformation through cold rolling to 5 or 10%. This alloy was aged for 2, 7 or 21 days at 170ºC.

Alloy	Cu	Mg	Mn	Si	Fe	Cu/Mg
Alloy 1: Al-1.3Mg-0.07Cu-0.4Mn	0.07	1.34	0.44	0.19	0.19	0.05
Alloy 2a: Al-3Mg-0.2Cu-0.1Mn	0.18	3.16	0.12	0.12	0.10	0.06
Alloy 2b: Al-3Mg-0.2Cu-0.1Mn	0.17	3.09	0.12	0.14	0.09	0.06
Alloy 3: Al-1.2Mg-1.2Cu-0.2Mn	1.19	1.19	0.20	0.03	0.02	1.00
Alloy 4: Al-1.5Mg-1.8Cu-0.2Mn	1.82	1.49	0.20	0.02	0.02	1.22

Table 1 Chemical composition of alloys (at%)

Alloy 2a and 2b are different batches of plate with identical target composition. Alloy 2a was solution heat treated at 550°C for 30 min, and subsequently quenched. Ageing was carried out at 180°C for a range of times between 1 and 8 h. DSC samples were prepared from the heat treated samples. Alloy 2b was produced through casting, followed by hot and cold rolling (see [41,42]). DSC samples of alloy 2b were resolution treated at 460°C and aged at 140 and 160°C.

Alloys 3 and 4 were produced as hot rolled plate. DSC samples were re-solution treated at 495°C for 30 min, quenched into room temperature water, weighed and introduced into the calorimeter. DSC runs started three minutes after the quenching.

All DSC samples were disc shaped (5 mm diameter, approximately 1 mm thick). DSC measurements were performed using a Perkin-Elmer calorimeter Pyris 1 DSC, with pure nitrogen purge gas as protective gas atmosphere. Heating rates from 2.5 to 150°C/min was used. The calorimeter was calibrated with an Indium standard at all block temperatures used (-30, -50, -100 and -140°C). All DSC traces were corrected by subtracting a baseline obtained from a DSC run with empty aluminium pans. Further corrections for imperfections of the DSC as well as correction for the heat capacity contribution not related to reactions of the samples is needed [43]. The optimum choice for this correction is alloy dependent and was considered in [44]. For the Cu-lean

alloys 1 and 2, further correction was achieved by subtracting a linear function of T fitted to the initial part of the curve, where no reactions are thought to occur. Alloys 3 and 4 were further corrected by a second order polynomial which described the combined effect of heat capacity difference of the sample and reference and baseline fluctuations. The coefficients of the second order polynomial were fitted by assuming that the heat effects due to reactions were zero at the following three points: (1) at the initial part of the curves where no reaction occurs; (2) at the completion of the S dissolution effect; and (3) at the point where the precipitation effect of the clusters ends and the dissolution effect of the clusters starts. Thus all DSC curves presented represent heat flows caused by reactions, which are directly related to enthalpy changes:

$$\Delta H = \int_{T_1}^{T_2} c_p dT \qquad (18)$$

where c_p is the heat flow measured by the DSC (the heat capacity at constant pressure) between the selected temperatures T_1 and T_2. (Selected DSC data on alloys 3 and 4 is taken from [45])

Possible experimental error in the temperature determination in DSC experiments is mainly due to sample variability and instrument calibration. The overall accuracy is typically about 1 to 2ºC. The main source of inaccuracy for the determination of the part of ΔH due to reactions is the choice of the points in the baseline correction and to a lesser extend sample variability and instrument calibration. Typical accuracies are in the order of 3% or 0.2J/g, whichever is the higher.

Course intermetallic phases (typically larger than 100nm) in Alloys 1-4 were studied in a Jeol 6500F Field Emission Gun Scanning Electron Microscope (FEG-SEM) equipped with Energy Dispersive Spectrometer (EDS) using mechanically ground and polished samples.

Results and Analysis

Thermodynamic data

As a result of the very low Cu content, DSC thermograms of alloy 1 generally showed very weak thermal effects. Samples aged for 2 days at 170°C show a small endothermic effect which peaks at 220ºC (curves not presented). Due to the very low heat flows and slight baseline instability the DSC curves of alloy 2 aged at 180°C (Fig. 3) become progressively more erratic beyond about 250ºC. However up to about 250ºC the DSC thermograms of alloy 2 are consistent and when aged for 4 to 48h at 180°C the alloy, showed a substantial endothermic effect peaking at 230ºC. This effect is seen to develop gradually during ageing for 1, 4 and 8 h, reaching a maximum heat content after 8h. This gradual development of the endothermic effect relates to a gradual increase in G of the samples on ageing. TEM data on the same alloy shows that after 4 and 8 h of ageing, coherent nanometer-sized needle and lath shaped particles are present [46,47]. After 1 h ageing these precipitates could not be detected in the TEM. At this stage of the ageing the DSC thermograms

show a dissolution effect that peaks at about 210ºC, with a heat content that is substantially lower than that obtained after 4 and 8 h.

DSC curves of the solution treated alloy 2B aged at 140°C are presented in Fig. 4. This data shows that in as quenched samples an exothermic reaction occurs at about 120 to180°C. When aged at 140°C this exothermic reaction disappears and the heat evolved in the endothermic reaction between 220°C and 270°C increases. The ageing treatments considered here are less severe than the 4 and 8 h of ageing at 180°C in which ordered nano-scale precipitates were detected in alloy 2. Thus, these precipitates should not form during ageing at 140°C. The effects observed in Fig. 4 are interpreted to be due to the formation of co-clusters at about 120 to180°C, whilst the endothermic effect is thought to be due to the dissolution of co-clusters with in the latter stages some transformation of co-clusters a phase with long range order, probably the rod/lath shaped particles observed by Kovarik et al [23].

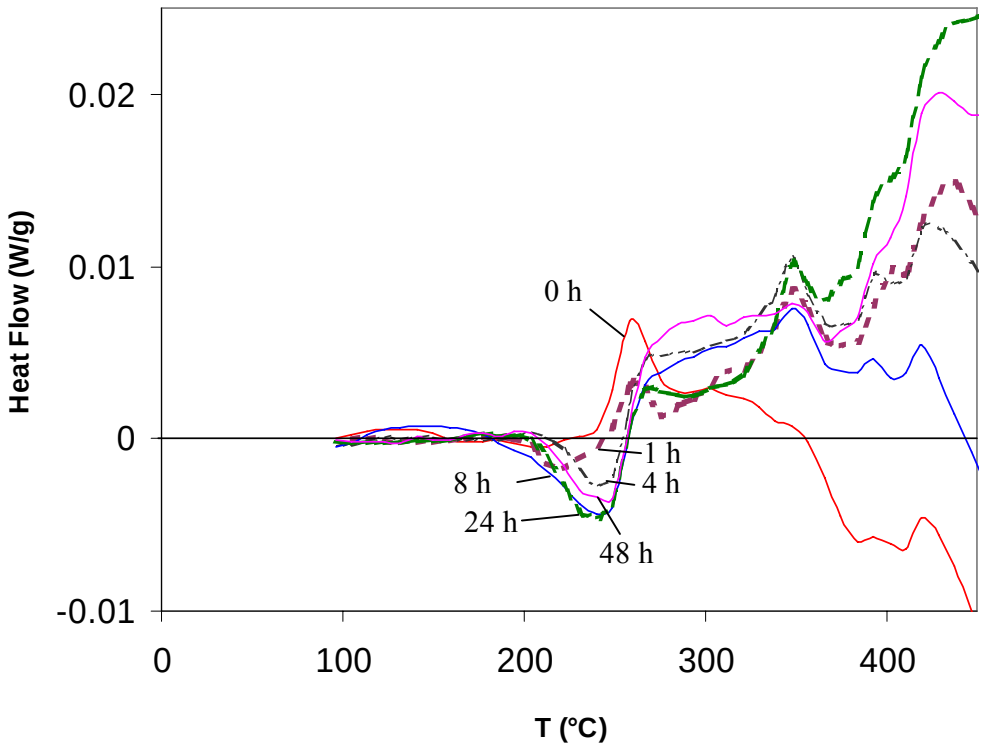

Fig. 3 DSC thermograms of solution treated alloy 2 Al-3.2Mg-0.18Cu after ageing for 0, 1, 4, 8, 24 and 48h at 180°C.

DSC curves of the solution treated Al-1.2Mg-1.2Cu alloy (alloy 3) at different heating rates are presented in Fig. 5a. These thermograms show heat effects that have heat contents well in excess of those observed in alloy 1 and 2. Consistent with the well-known theory of thermally activated reactions [48], heat effects in these curves shift to higher temperatures with increasing heating rate. The end temperature of exothermic effect (T_e), which also increases with temperature, reflects the stage at which the driving force for further reaction has decreased to zero [49]. This is the stage at

which the average composition of solute atoms in the Al-rich phase has reached the metastable solvus. As T_e increases with heating rate, and the solvus concentrations increase with temperature, the total heat contents of the exothermic effects decrease with increasing heating rate [50]. On ageing for up to 24 h at room temperature, the first exothermic effect in the DSC curves of the solution treated alloy 3 (Al-1.2Cu-1.2Mg) gradually disappears. 3DAP analysis of these alloys presented elsewhere [7,51] shows that whilst immediately after quenching the Mg atoms are randomly distributed, Mg atoms become clustered, and from analysis of clusters that are larger than about 10 atoms, the formation of Cu-Mg co-clusters is identified. No other phases can be identified, and hence the low temperature exothermic reaction is attributed to the formation of Cu-Mg co-clusters. DSC curves of the solution treated alloy 4 (Al-1.8Cu-1.5Mg) at different heating rates are presented in Fig. 5b. These thermograms show heat effects at similar positions to those in alloy 3, whilst the heat contents of the effects are on average about 40% larger. 3DAP analysis similar to that described for alloy 3 indicated that also for alloy 4 the low temperature exothermic effect was due to the formation of Cu-Mg co-clusters [7].

The measured heat contents of the effects and isothermal ageing temperatures for the alloys are presented in Table 2. A range of data on $\Delta Q(T_e)$ presented in the literature [52,53,54] on a number of alloys is also included in this table.

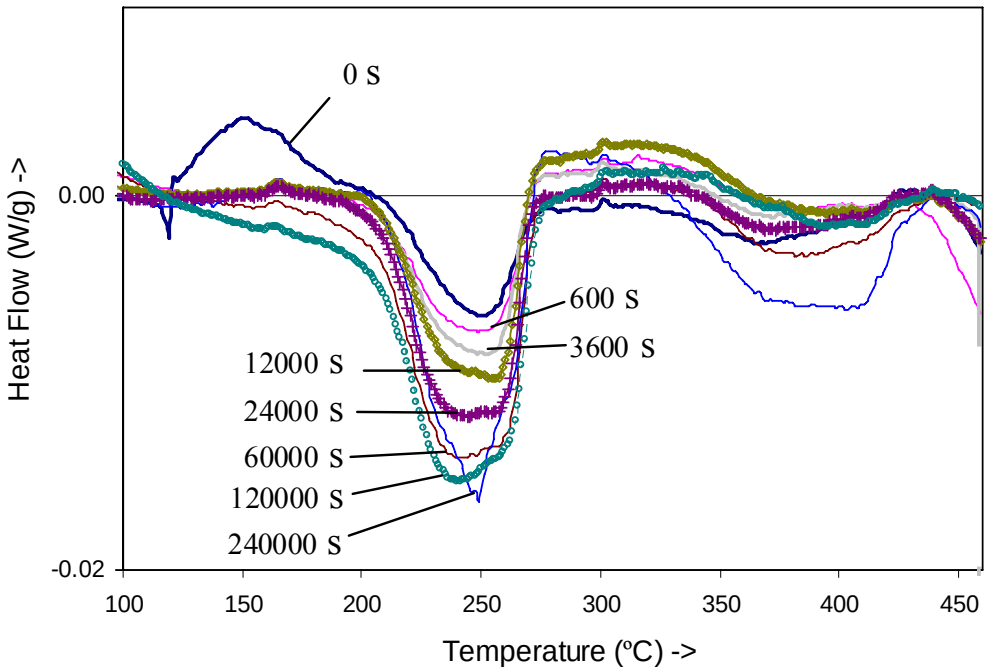

Fig. 4 DSC curves of the solution treated alloy 2B (Al-3.1Mg-0.17Cu) after solution treatment and after ageing for up to 240ks (60.7h) at 140°C.

Experiment	Reference	x^g_{Cu}	x^g_{Mg}	x^g_{Mn}	T_e (ºC)	ΔQ (J/g) measured	ΔQ (J/g) predicted
IC	Zahra et al [52]	0.0025	0.047	0.0007	60	3.5	3.15
DSC exo	Verlinden & Zahra [53]	0.0025	0.047	0.0007	195	2.9	2.72
IC	Zahra et al [52]	0.0023	0.033	0.0004	60	3.5	2.89
IC	Zahra et al [52]	0.0040	0.033	0.0008	60	6	5.04
DSC exo	Verlinden & Zahra[53]	0.0040	0.033	0.0008	180	4.4	4.56
IC	Zahra et al [52]	0.0090	0.014	0.0000	30	11.7	11.4
IC	Zahra et al [52]	0.0110	0.017	0.0000	30	13.5	13.9
DSC exo	This work	0.0007	0.013	0.0000	170	0.2	0
DSC exo	This work	0.0007	0.013	0.0000	170	0	0
IC	Zahra et al [52]	0.0025	0.047	0.0007	0	0	3.16
IC	Verlinden & Zahra [53]	0.0040	0.033	0.0008	0	0	5.06
DSC exo	Charai et al [54]	0.0087	0.014	0.0000	150	9.4	9.81
DSC exo	Charai et al [54]	0.0090	0.015	0.0000	165	9.3	9.77
DSC exo	This work	0.0121	0.012	0.0020	111	14.1	12.5
DSC endo	This work	0.0018	0.030	0.0000	180	2	1.74
DSC	This work	0.0018	0.030	0.0000	215	0	0.00
DSC endo	This work	0.0018	0.030	0.0000	180	0.5	0.00
DSC endo	This work	0.0017	0.032	0.0012	140	2.0	1.95
DSC endo	This work	0.0017	0.032	0.0012	200	0.7	1.45

Table 2 Magnitude of the heat contents of exothermic precipitation effect and heat contents of endothermic dissolution effect (ΔQ) with gross compositions ($x^g_{Cu}, x^g_{Mg}, x^g_{Mn}$). In the first column 'DSC exo' stands for an exothermic effect observed in a linear heating experiment, 'DSC endo' stands for an endothermic effect observed in a linear heating experiment, IC stands for an exothermic effect observed in an isothermal calorimetry experiment. T_e stands for the end temperature of the exothermic effect in a 'DSC exo' experiment, or the ageing temperature in a 'DSC endo' experiment, or the isothermal ageing temperature during the IC experiment.

Comparing thermodynamic data with the model

To compare the measured ΔQ data with the regular solution model for dimers, model predictions were made using Eqs. 1-3 with Eqs. 7-9. In order to achieve these model predictions we first needed to determine $\Delta H_{A\text{-}B}$. From each data line in Table 2 a value of $\Delta H_{A\text{-}B}$ can be obtained, we take $\Delta H_{A\text{-}B}$ as the average from the experiments that are expected to yield the highest accuracy: DSC experiments at 5-40ºC/min for the alloy with the highest $x_{Cu}+x_{Mg}$. This provides $\Delta H_{A\text{-}B}$ = 34.5±0.5kJ/mol. The predicted ΔQ values are presented in Table 2 and graph of predicted vs measured values of ΔQ considering all reactions which completed within 20 min for T_e >100ºC and completed within 7 days for $T_e \leq$60ºC is provided in Fig. 6. Plots of ΔQ vs T_e for alloys 3 and 4 are provided in Fig. 7. The correspondence between the regular solution model for dimers and the thermodynamic data obtained from calorimetry is excellent for all alloys.

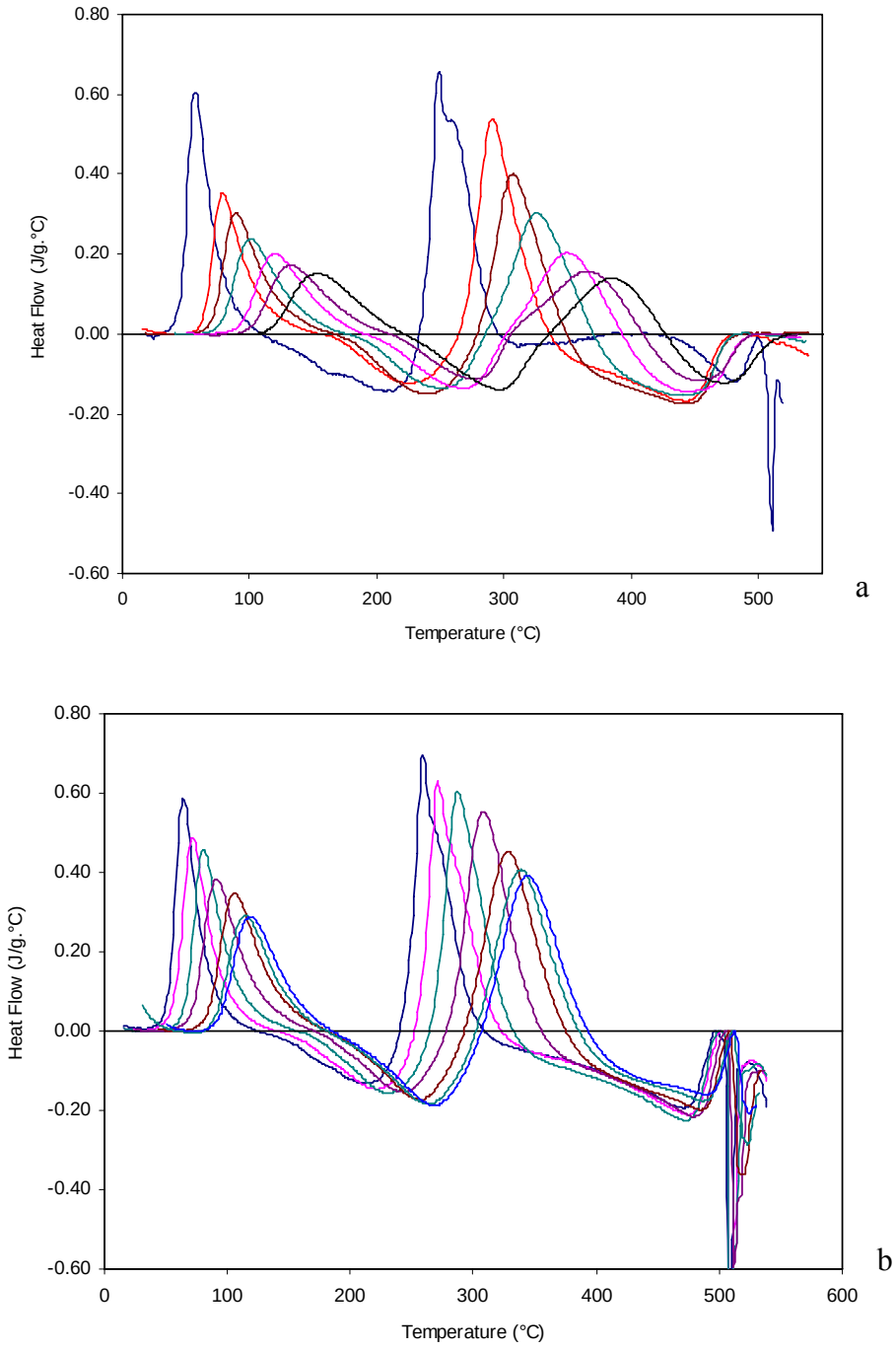

Fig. 5 DSC curves of a) the solution treated alloy 3 (Al-1.2Cu-1.2Mg) at (from left to right) heating rates 2.5, 10, 20, 40, 80, 120 to150 K/min; and b) the solution treated alloy 4 (Al-1.8Cu-1.5Mg) at (from left to right) heating rates 5, 10, 20, 40, 80, 100 and 120 K/min.

The validity of the thermodynamic model was further checked by comparing predictions for ΔQ using the more general equation Eq. 5 and optimising a, $\Delta H_{\mathrm{MmAaBb}}$ and C (b is fixed at 1, this is not a limitation as there are only 3 independent parameters). Best fits were obtained with a close to 1, which confirms that clusters have Cu:Mg ratios close to 1. Solvus predictions with optimised a, ΔH_{c}

and *C* for the alloys were within about 2ºC of the one obtained with the regular solution model for dimers.

Additional DSC experiments were performed on two alloys that are right at the limit of stability of co-clusters at typical formation temperatures: Al-0.08Cu-1Mg (at%) and Al-0.08Cu-2Mg (at%). For these alloys predicted heat evolution are 0 and 0.4J/g, respectively. Observed heat of dissolution of co-clusters are right at the detection limit, at 0.2±0.2 J/g averaged for the two alloys. These observations should be compared with the data for alloy 2b, for which co-cluster formation and dissolution was readily observed. Thus, these observations provide further support for the model predictions on stability limits of co-clusters for these alloys with very low Cu content.

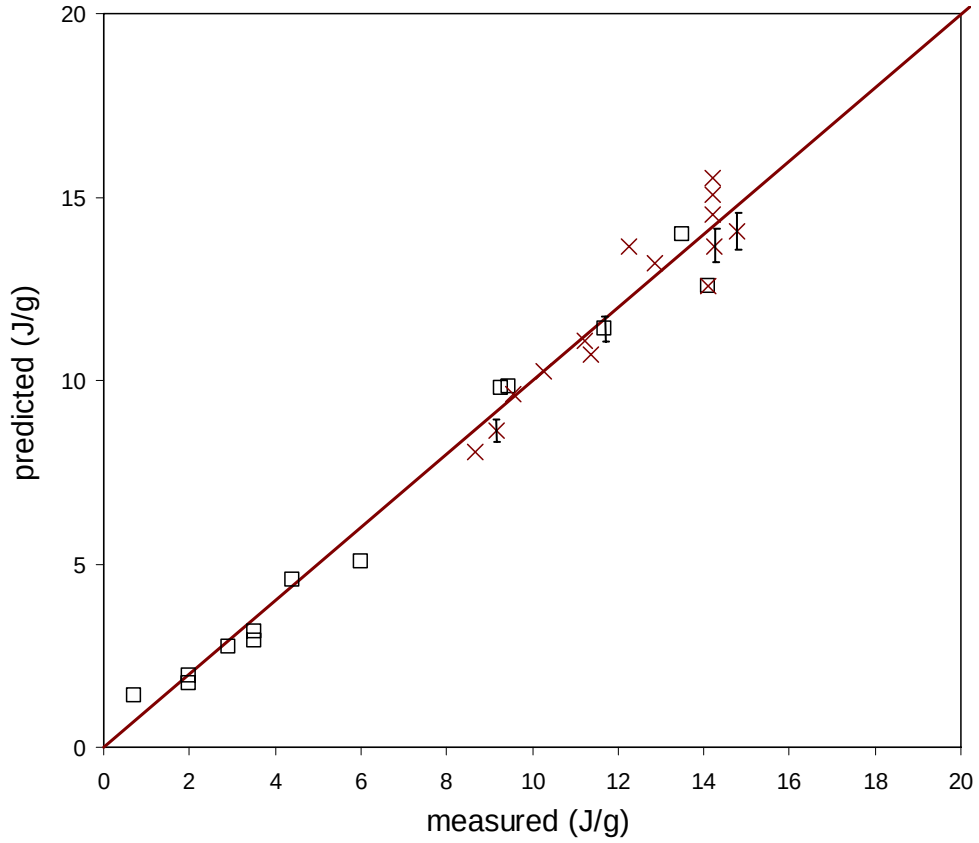

Fig. 6 Measured vs. predicted ΔQ from calorimetry experiments for a range of Al-Cu-Mg alloys. a=1, ΔH_c=34.5kJ/mol. × : DSC data on alloys 3 and 4; □ : all other data.

Considering the typical measurement error, the level of agreement between calorimetry data and predictions of the thermodynamics based on a regular solution model in Fig. 6 and Fig. 7 is excellent. These figures contain thermodynamic data for a wide range of alloys for the full range of temperatures at which co-cluster formation is normally observed (20 to 200ºC). To prove the regular solution model is not just a fortuitous fit but physically realistic, we will show in the Discussion section that the present interpretation is consistent with published microstructural data.

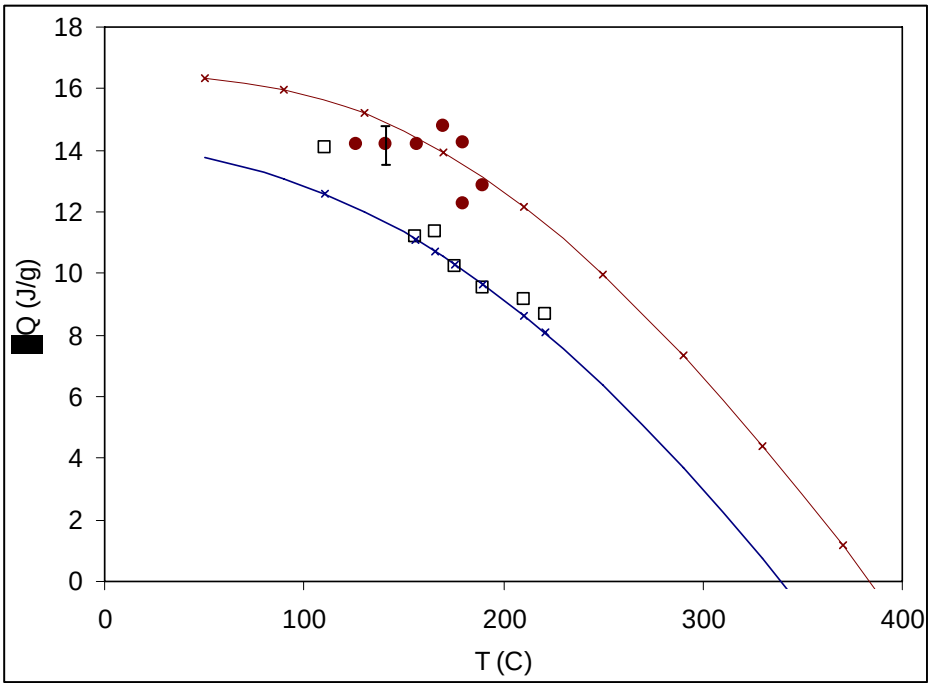

Fig. 7 Measured ΔQ (symbols) and predicted ΔQ (lines) as a function of end temperature for alloys 3 and 4. a=1, ΔH_c=34.5kJ/mol.

Strength and hardness data

The yield strength of an alloy that contains co-clusters is dominated by the contribution due to clusters, with further minor contributions due to grain boundaries, dislocations and solute in the Al rich phase. A general approximation of the superposition of strengthening mechanisms is [55]:

$$\begin{aligned}\sigma_y &= \sigma_{gb} + M\left(\tau_{sol} + \tau_d + \tau_{cl}\right) \\ &= \sigma_{gb} + M\left(\tau_{sol} + \tau_d + (\Delta\tau_{sro} + \Delta\tau_m + \Delta\tau_{ch})\right)\end{aligned} \tag{19}$$

where σ_{gb} is the contribution due to grain boundaries τ_d is due to stored dislocations (introduced by working) and τ_{sol} is due to dissolved elements. The method for obtaining σ_{gb} is outlined in [55], it provides σ_{gb} values that are less than 1 MPa for the relatively coarse grained alloys considered here. In the alloys considered, τ_d is zero for solution treated and aged alloys and for T351 (solution treated stretched and aged alloys) it is obtained from the model outlined in [56], which provides τ_d values of about 5 MPa. τ_{sol} is obtained form the model outlined in [57]. To verify the model we will compare yield strength predictions with data for a range of solution treated and subsequently aged Al-Cu-Mg alloys. (Strength of rolled Al-Cu-Mg alloys is anisotropic. Where available we will use the average of L and LT tests; if only L is available we will consider that the average of L and LT yield strengths, $\sigma_{y,L}$ and $\sigma_{y,LT}$, is about 0.95 $\sigma_{y,LT}$ [58].) The results, presented in Table 3, show a very good correspondence: the typical accuracy (root mean square error) is 11 MPa for data ranging from 110 to 350MPa. This limited level of deviations is thought to be mostly due to small uncertainties not related to the present strength model that include uncertainties in alloy

composition (a 0.1wt% change in Cu content causes 6MPa change in predicted σ_y), limited measurements inaccuracies and the anisotropy of yield strength introduced by texture of rolled alloys.

x^g_{Cu} (at)	x^g_{Mg} (at)	σ_y measured (MPa)	σ_y modelled (MPa)	T (ºC)	Ref
0.0179	0.0139	315	295	25	This work
0.0119	0.0117	265	273	25	This work
0.0106	0.0160	250	262	30	Wil [59]
0.0106	0.0128	255	258	20	Pol [60]
0.0050	0.0170	150	148	150	Rav [61]
0.0080	0.0170	200	204	150	Rav [61]
0.0110	0.0170	245	246	180	Rav [61]
0.0187*	0.0160*	325	343*	25	ASM [63]
0.0183	0.0148	348	346	25	Sri [64]
0.0179	0.0145	328	316	25	This work
0.0025	0.0450	130	140	180	Rat [65]
0.0024	0.0320	95	114	180	Cou [66]
0.0022	0.0427	112	126	180	Cou [66]
0.0169	0.0108	277	289	25	Fin [67]

* The median 2024 composition with 0.1 wt% Fe is assumed.

Table 3 Predicted and measured yield strengths of various solution treated and subsequently aged Al-Cu-Mg alloys. Ageing is conducted to a state where co-cluster formation is completed: 4 to 10 days at 25°C and about 5 min at 150 and 180°C. Data obtained for this work and from [59] Wil, [60] Pol, [61,62] Rav, [63] ASM, [64] Sri, [65] Rat, [66] Cou, and [67] Fin.

Discussion

Comparison of the thermodynamic model for dimers (regular solution model) and the strength model with calorimetry and yield strength data of well over a dozen Al-Cu-Mg alloys spreading over a wide range of compositions shows an excellent correspondence, with any remaining deviations likely to be mainly (or exclusively) caused by limited experimental errors. This has been achieved through determining just one parameter $\Delta H_{A\text{-}B}$. For other alloy systems that may contain co-cluster no consistent set of calorimetry and strength data could be found and hence, at present, we can not test the models for other alloys. However it appears clear from the present model that for a range of ternary or higher order alloys that are processed though a supersaturated solid solution involving two or more alloying elements decomposition will progress through a co-cluster stage. In the following we will focus our discussion on co-clusters in the Al-Cu-Mg system.

In the following discussion we will first discuss possible variants of the thermodynamic model, cluster size and cluster composition. Secondly, we will aim to show that all published microstructural data and quantum mechanic modelling is consistent with the present models. Thirdly we will consider possible other strengthening models. And finally we will show how the models can quantitatively explain the phenomenon of secondary ageing in Al-Li-Cu-Mg alloys.

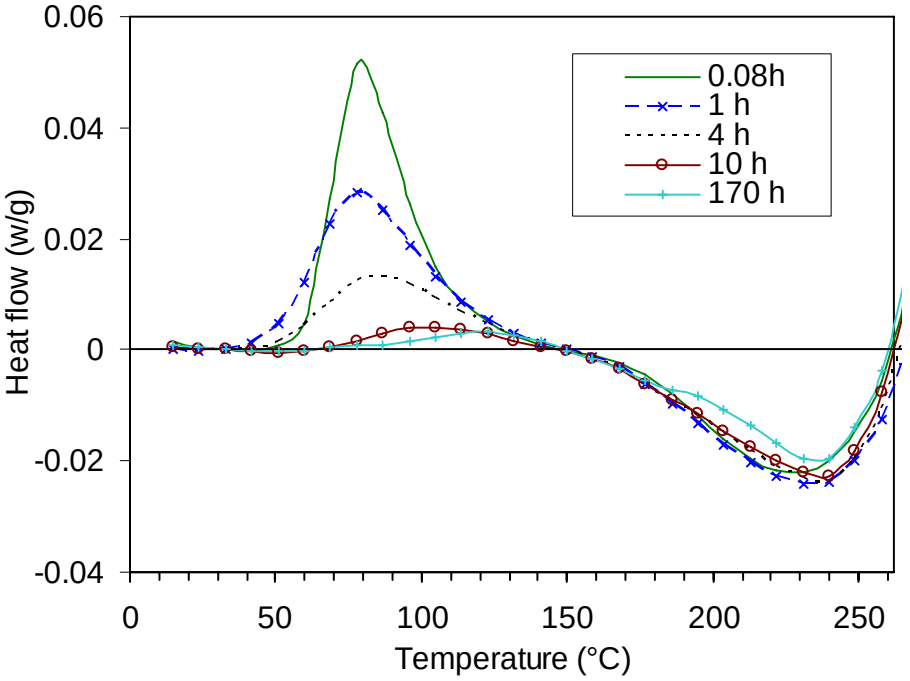

Fig. 8 DSC thermograms for quenched and subsequently room temperature aged Al-1.2at%Cu-1.2at%Mg alloy. Depicted are thermograms after ageing times of (in order of decreasing exothermic heat effect) 0.08, 1, 4, 10 and 170h.

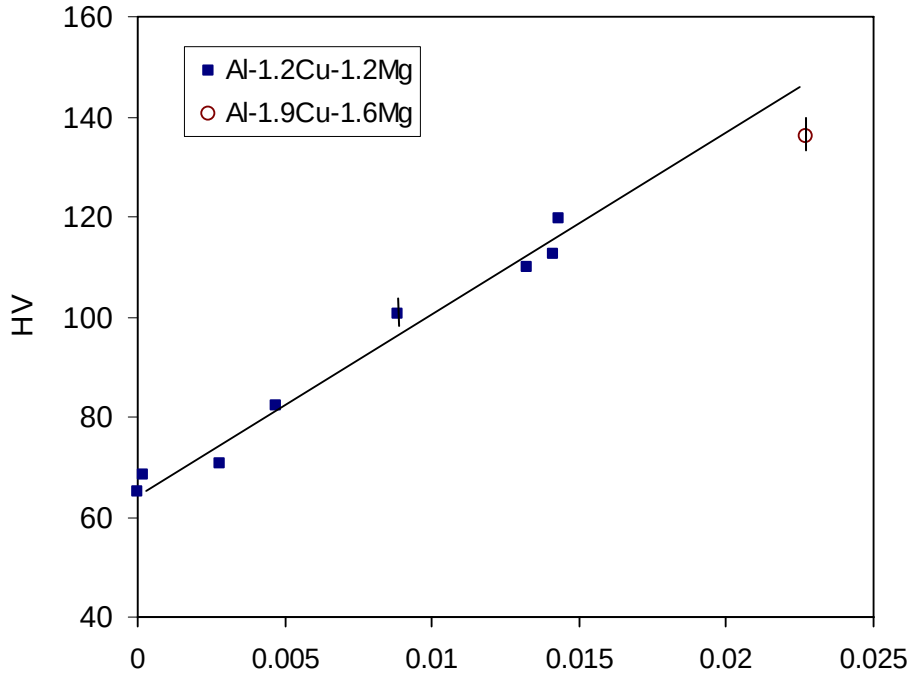

Fig. 9 Measured Vickers hardness vs the fraction of Cu and Mg atoms in co-clusters (for ΔH_c=34.5kJ/mol).

Cluster composition and further evolution

As the fitting of the broader thermodynamic model (Eq. 5) provides *a:b*=1, the basic unit element of the co-cluster is $Cu_1Mg_1Al_p$ or multiples of these. In terms of the regular solution model this leaves open various possibilities, for instance complexes of 2 Cu atoms with 2 Mg atoms, with the Cu and Mg atoms not situated as nearest neighbours but separated by a certain number of Al atoms. Examples are given in Fig. 1. However, the excellent correspondence of the thermodynamic model for dimers and the strengthening model for dimers indicates that the main reaction involves the formation of the Cu-Mg dimers: one Cu and one Mg atom in nearest neighbour positions. However this in itself does not exclude the possibility of larger co-clusters; and in fact all co-cluster constellations where ΔH for co-cluster formation is essentially related to a chain of bonds such as illustrated in Fig. 1 is consistent with the measured enthalpy changes and strength data. Isothermal calorimetry data shows that exothermic heat evolution during room temperature hardening peaks during the hardening, and reduces to zero by the time the hardness stabilises after about 48 h at room temperature. The latter, whilst consistent with the present models for dimers as well as extended chains where ΔH for co-cluster formation is essentially related to a chain of bonds, also indicates that any further growth of co-clusters does not have a significant impact on the enthalpy of the alloy. Hence, the occasional occurrence of larger co-clusters (larger than 10 atoms, in some cases larger than 100 atoms) should be considered as a coagulation of smaller co-clusters; with the coagulation not influencing the strength or ΔH to a significant extend. In these coagulated dimers some relaxation of the atomic positions will occur and the model for a needle/lath like phase appearing after 24-96h at 180ºC [23] can in fact be considered as a coagulation of dimers like in Fig. 1c with some relaxation of atoms positions.

Nanostructure data and quantum mechanical modelling

Whilst atom probe analysis can not show the existence of individual dimers, data is fully consistent with the above model. In particular, APFIM on Al-Cu-Mg based alloys show that [7]:

- during ageing after solution treatment co-clusters are formed
- clusters of sizes that can be reliably detected (typically more than ~10 atoms) do occur but only a small fraction of the Cu and Mg atoms are associated with these larger clusters
- the larger clusters have Cu:Mg ratios that vary, with a median value of about 1

Thus atom probe data is fully consistent with the present models on dimer formation, and the experiments show exactly the features that can be expected. Also Nuclear Magnetic Resonance (NMR) [10] and positron annihilation lifetime spectroscopy (PALS) [13] are sensitive to Cu-Mg dimer formation. NMR and PALS studies on Al-Cu-Mg alloys have indeed shown that after the rapid hardening reaction the chemical environment of Cu atoms has changed [10,13], but the published analysis of the experiments fails to identify what this change entails. Microstructural data for two broad groups of experiments (near room temperature and near 150ºC) are presented in Table 4. The table includes TEM and selected area diffraction (SAD) on an Al-4wt%Cu-1.5wt%Mg alloy that was solution treated, quenched and aged at room temperature for about a year. This confirmed that no additional diffraction phenomena are observed in SAD and no precipitates can be observed in bright field TEM imaging.

	Alloy (at%)	T (°C)	t	experiment	observation
this work	Al-1.9Cu-1.6Mg	25	10000h	TEM	no precipitates resolvable
this work	Al-1.9Cu-1.6Mg	25	10000h	SAD	no diffraction effects due to precipitates
Starink et al [7]	Al-1.9Cu-1.6Mg and Al-1.2Cu-1.2Mg	25	0-200h	calorimetry	H decreases strongly*, H stabilises at about 2h
Starink et al [7]	Al-1.9Cu-1.6Mg and Al-1.2Cu-1.2Mg	50	0-200h	calorimetry	H decreases strongly*, H stabilises at about 15h
Fink et al [67]	Al-1.7Cu-(0.5-1.5)Mg	30	0-10h	dilatometry	expansion
Fink et al [67]	Al-1.7Cu-(0.5-1.5)Mg	31	0-10h	dilatometry	increased resistivity
Staab et al [12]	Al-2.0Cu-1.8Mg-0.6Mn	25	120h	XANES	consistent with Cu-Mg bonds, not with Cu in solution, or Cu-Cu clustering;
Starink et al [7]	Al-1.2Cu-1.2Mg	25	0.5-3.5h	3DAP - statistical	onset of co-clustering happens between 1 and 2 h
Starink et al [7]	Al-1.2Cu-1.2Mg	25	2-30h	3DAP - imaging	clusters with more than 7 atoms are detectable, but numbers insignificant
Bastow [10]	Al-1.05Cu-1.7Mg	21	0-645h	NMR	change chemical environment of atoms from ~10 min to ~30h
Ringer et al [21]	Al-1.1Cu-1.7Mg	20	24h	hardness	hardening to plateau completed at 24h
Starink et al [7]	Al-1.9Cu-1.6Mg and Al-1.2Cu-1.2Mg	25	0-200h	hardness	hardening to plateau occurs between 0.01 and 2h
Reich et al [68]	Al-1.7Mg-1.1Cu	150	1 min	TEM	no precipitates resolvable at 1 min
Reich et al [68]	Al-1.7Mg-1.1Cu	150	1min	SAD	no precipitates at 1 min
Reich et al [68]	Al-1.7Mg-1.1Cu	150	1min	Hardness	hardness reaches plateau within 1 min
Reich et al [68]	Al-1.7Mg-1.1Cu	150	1min	3DAP	Cu:Mg ratio in larger clusters about 3:5
Reich et al [68]	Al-1.7Mg-1.1Cu	150	1-60min	3DAP	Cu-Mg co-clusters detected at 5min, not detected at 1min
Ringer et al [20]	Al-1.7Mg-1.1Cu	150	5min	AP	Cu-Mg co-clusters detected at 60 min
Ringer et al [20]	Al-1.7Mg-1.1Cu	150	5min	TEM	no precipitates resolvable at 5 min
Ringer et al [21]	Al-1.1Cu-1.7Mg	130	linear heating ~10min	calorimetry	H decreases strongly*
this work	Al-1.2Cu-1.2Mg	120	linear heating ~10min	calorimetry	H decreases strongly*, H stabilises at 120°C during heating at 10K/min

* change in *H* is about half of that due to formation of the equilibrium phase, the S phase.

Table 4 Microstructural data on the two broad groups of experiments: ageing experiments performed at room temperature and near 150°C, for times up to about 10 times the time required to reach the hardness plateau.

The data in Table 4 is fully consistent with the present models for co-clusters, with the exception of one observation by Reich et al [68] who failed to detect Cu-Mg co-clusters in a sample aged for 1 min at 150ºC (by they do detect them after 5 min). In the absence of any data supporting this one finding we consider the weight of evidence clearly supports the present models, and we will disregard this one finding. We further investigated literature on TEM, HREM, SAD in TEM, APFIM, 3DAP, calorimetry, NMR and PALS experiments for ageing times within about 10 times the time to reach the plateau hardness (or time to stabilise the enthalpy) in about 50 papers (encompassing [7,12,19,20,23,**Error! Bookmark not defined.**] and references therein, and references [10,11,13,15-22,44,51,52,53,65]), and concluded that the present model is consistent with all the available data. In particular it should be noted that no microstructure investigation ever showed evidence for precipitates (other than co-clusters suggested by APFIM, 3DAP) for ageing times within about 10 times the time to reach the plateau hardness (or time to stabilise the enthalpy).

This assessment further indicates that the term GPB zones, associated with early decomposition and hardening in Al-Cu-Mg alloys in most of the pre 1995 papers cited in this work, does not reflect accurately the processes involved, and is ultimately obfuscating or, depending on which of the definition of GPB zones is used, even misleading.

Next the first principles model prediction (VSP) was assessed. A first principles total energy calculation (FP-CVM) of 4 atom tetrahedrons provides an enthalpy of mixing of 30kJ per mole Cu-Mg dimers [25]. This is in good agreement with the present model and analysis, and the small deviation can be due the limitations in accuracy provided by this 4 atom tetrahedrons calculation. We may also compare our results with the enthalpy of mixing for the coherent rod/lath-like structures formed in a later stage of the ageing (24-96h at 180ºC) in an Al-0.4at%Cu-3at%Mg alloy [23]. For the coherent rod/lath-like structures identified by Kovarik et al. [23], 5×5×1 and 6×6×1 supercell calculations determine an enthalpy of formation of 48 kJ per mol solute atoms in the GPB structure [23]. Thus these coherent rod/lath-like structures are more stable then the Cu-Mg dimers and should be considered a stage of the ageing of the alloys that is subsequent to the co-cluster formation.

An alternative treatment for thermodynamics of clusters suggested in the literature [24] involves a quasi-chemical model which takes nearest neighbour interactions into account. Analysis of this model showed that it can not explain all the experimental observations. Particularly, this model can not reconcile the observations that immediately after water quenching no Cu-Mg co-clustering is detected, with the enthalpy of formation of Cu-Mg co-clustering being of the order determined here.

Strength models for co-clusters: comparison with previous models

The present model for co-cluster strengthening indicates that the yield strength of alloys which contain only co-clusters as strengthening precipitates is in good approximation proportional to the amount of the co-clusters. This is different in previous models for co-cluster strengthening (and the vast majority of other precipitation strengthening mechanisms) which predict a square root of the amount (or square root of volume fraction) dependency. This allows us to test the model in the following fashion. We have performed hardness tests on an Al-1.2at%Cu-1.2at%Mg alloy during room temperature ageing for time t_{NA}, and also performed DSC experiments on samples of the same alloy subjected to the same natural ageing treatments. The DSC thermograms are presented in Fig. 8. The total change in heat released during the DSC experiment for each naturally aged sample, $\Delta Q(t_{NA})$, was measured and the change during ageing, $\Delta Q(t_{NA})$- $\Delta Q(t_{NA}=0)$, was determined. The latter difference, $\Delta Q(t_{NA})$- $\Delta Q(t_{NA}=0)$, should be proportional to the amount of co-clusters formed during ageing, and the amount of co-clusters thus obtained is plotted as a function of the hardness in Fig. 9. (One further data point for Al-1.9at%Cu-1.6at%Mg aged for 100 h is added.) The graph of f vs HV shows a linear correlation, which further supports the present strengthening model, whilst clearly showing strength increments are not proportional to $f^{1/2}$.

In several works (e.g. [38]), including some from the present group (e.g. [7,57]), strengthening by co-clusters has been modelled by considering only modulus hardening is effective. Eq. 14 (the simplified form for modulus hardening) was applied in these works, and through fitting of μ_{cl}

generally good results were obtained. Whilst the present work indicates that this approach is mistaken in terms of the identification of the fundamental processes at work, it can be seen that fitting a value for μ_{cl} higher than the actual value of μ_{cl} can provide an effective fit for a limited range of data.

We further note that the present co-cluster hardening model provides an explanation for a range of observations in ternary and higher order alloys. For example, through combining Eqs. 6, 9, 13 and 19, and assuming solution strengthening is substantially less than co-cluster strengthening, the increase in strength of an alloy on formation of co-clusters is proportional to the change in enthalpy during co-cluster formation. Such a proportionality is found for Al-1.7%Li-Cu-Mg alloys that were exposed for 1000 h at 70ºC following an solution treating and an ageing treatment at 150ºC [69] and the proportionality constant is consistent with the present model. This secondary ageing treatment does not cause any changes in microstructure that can be detected by TEM. This shows that the magnitude of secondary age hardening in this alloy can be quantitatively explained by the formation of co-clusters.

It is also noted that the present models show that co-clusters impart both a significant strength and, as a result of the strong decrease resistance to dislocation movement on passage of a one dislocation, they also cause an unusually high propensity for shear localisation. In fatigue loading conditions the shear localisation would cause a propensity for roughness induced crack closure (RICC) [8], provided grains are reasonably large. Thus an alloy with high amounts of co-clusters would be ideal for applications requiring fatigue resistance and strength, and optimisation of these mechanical properties would be achieved through maximising the co-cluster content. Published calorimetry and APFIM work on a range of alloys have indicated that of the light f.c.c. metallic alloys Al-Cu-Mg have the highest co-cluster content. From this information we can now determine the composition of the optimum alloy for specific strength and fatigue resistance in the following way:

- Our model shows that underaged Al-Cu-Mg alloys with Cu:Mg content close to 1 and Cu and Mg solute levels close to the maximum solubility should provide maximum co-cluster content. Using phase diagrams of ternary alloys this indicates an Al-1.6Cu-1.6Mg alloy.
- We also consider that Mn additions at levels of about 0.2 at% are effective in promoting recrystallisation through formation of T-$Al_{20}Cu_2Mn_3$ dispersoids [26], which are to a large extend not dissolvable in the Al-rich phase. Thus Mn additions will remove some Cu from solid solution and also Fe impurities will remove some Cu from solid solution (through formation of ω-Al_7Cu_2Fe); and it is clear that the best alloys for specific strength and fatigue resistance (and commercially viable impurity levels) should be Al-1.8Cu-1.6Mg-0.2Mn-0.05Fe alloys in underaged conditions.

The latter compositions and heat treatment are essentially identical to 2x24-T3 alloys, which are dominant in applications requiring a high specific strength and fatigue resistance, such as airplane fuselage and lower wing. Thus this analysis provides a rationale for alloy optimisation, linking atomic scale processes to properties at the component scale (wings and fuselage).

Conclusions

A thermodynamic model for co-clusters based on a single interaction energy of dissimilar nearest neighbour interaction energy is presented. Also a model for the strengthening due to these co-cluster dimers is derived. The model includes a new treatment of (short-) order strengthening relevant to these co-clusters and further encompasses modulus hardening and chemical hardening. Evaluation shows that in general (short-) order strengthening will be the main strengthening mechanism. The model is tested against data on Al-Cu-Mg alloys. It is shown that:

- The thermodynamic model can fully explain published and new data on the heat evolution due to co-cluster formation. The Cu-Mg interaction enthalpy $\Delta H_{A\text{-}B}$ is determined as 34.5±0.5 kJ/mol.
- The models can quantitatively predict the very first stage of hardening and associated heat evolution in Al-Cu-Mg alloys with Mg:Cu ratio between 20 and 0.5, and Cu contents between about 0.1 and 2 at%. The process of co-cluster formation is consistent with published data on microstructural evolution for relevant Al-Cu-Mg alloys.
- The model is successfully tested against data on strength and hardness of a wide range of Al-Cu-Mg alloys treated at temperatures between 20 and 220ºC.
- The term GPB zones, often associated with early decomposition and hardening in Al-Cu-Mg alloys, does not reflect accurately the processes involved, and is ultimately obfuscating or, depending on which of the definition of GPB zones is used, even misleading.
- Co-cluster formation involving dimers causes strength increments that are in good approximation proportional to the change in enthalpy of the alloy, and the proportionality constant is derived. This proportionally is seen in Al-Li-Mg-Cu alloys exposed at 70ºC, which strongly indicates that strengthening during low temperature exposure is due to formation of 2 atom co-clusters.

Acknowledgements

The following people are gratefully acknowledged: Ms. A. Dion, and Drs J.L. Yan, Z. Zhu and N. Gao for performing selected DSC experiments, Dr N. Gao for performing tensile tests on a 2024 alloy, Dr G. Mahon for thermomechanical processing of Alloy 2b, Drs G. Mahon, S. Court and L. Kovarik for discussions on low Cu Al-Mg-Cu-Mn alloys. QinetiQ (Farnborough, UK), Alcan (former Banbury Labs), Airbus UK and Prof M.J. Mills and Dr L. Kovarik are gratefully acknowledged for providing alloys.

Appendix: Undissolved intermetallics

Insoluble or undissolved particles and dispersoids, such as ω-Al_7Cu_2Fe, S-Al_2CuMg, T-$Al_{20}Cu_2Mn_3$, $Al_{12}(Fe,Mn)_3Si$ and $Al_6(Fe,Mn)$, which form during solidification or homogenisation, can be present in Al-Cu-Mg type alloys with Mn, Fe and Si additions and impurities [26,27]. Since the presence of ω, S and T phases will remove some Cu and Mg from the solid solution, it is necessary to calculate the effective solute concentration in the matrix after solution heat treatment.

The atomic fraction of undissolved ω-Al_7Cu_2Fe can be calculated based on the solubility of Fe in Al matrix, since the solubility of Fe is not significantly influenced by the additions of Cu or Mg [70]. At typical T_{SHT} for 2024 alloys, which is about 500°C, the maximum solubility of Fe in Al, x^e_{Fe}, is 0.0055 wt.% [71]. The amount of ω-Al_7Cu_2Fe in the alloy is then given by:

$$x_\omega = 10(x^g_{Fe} - x^e_{Fe}) \tag{20}$$

where x^g_{Fe} is the gross Fe content of the alloy. A similar treatment is applied to obtain the amount of $Al_{20}Cu_2Mn_3$. Based on the solvus of $Al_{20}Cu_2Mn_3$ in the Al-Cu-Mn system**,** at 500°C the solubility of Mn in Al with a Cu content of 4 wt%, is about 0.2wt% [70]. Thus the amount of T-$Al_{20}Cu_2Mn_3$ in the alloy is given by:

$$x_T = 25/3\,(x^g_{Mn} - x^e_{Mn}) \tag{21}$$

where x^g_{Mn} is the gross Mn content of the alloy.

In alloys for which the Cu and Mg contents are close to the solvus of S phase at the homogenising treatment, some undissolved S phase can be present. FEG-SEM investigation of alloys 2b, 3 and 4 showed that only alloy 4 contained undissolved S phase. DSC experiments showed that this alloy has an S phase solvus temperature within about 10ºC of the solution heat treatment temperature, T_{SHT}, whilst for the other two the difference is at least 30ºC. Thus we will consider that for all alloys with an S phase solvus temperature more than 30ºC below T_{SHT} all S phase is dissolved. For all other alloys we will estimate S phase content from available experimental data. An accurate calculation of the amount of S phase in alloy 4 is provided by the difference between the amounts of intermetallic phases detected in alloys 3 and 4. This provides V_S=0.009 for alloy 4. For the 2524 alloy in [60] we can estimate the amount of S phase from optical micrographs in [60] as about half that of our alloy 4.

The effective solute concentration in the matrix after solution treatment is obtained by from the difference of the gross content and the amounts in the undissolved phases.

References

1 E.V. Pereloma, A. Shekhter, M.K. Miller and S.P. Ringer. Acta Mater. 2004,52:5589.
2 E.V. Pereloma, I.B. Timokhina, K.F. Russell, M.K. Miller. Scripta Mater. 2006, 54:471.
3 Moody, MP; Stephenson, LT; Liddicoat, PV, Ringer SP. Microsc. Res. Techn. 2007, 70:258
4 Stephenson LT, Moody MP, Liddicoat PV, Ringer SP. Microsc. & Microanal. 2007,13:448
5 T. Honma, S. Yanagita, K. Hono, Y. Nagai, M. Hasegawa. Acta Mater. 2004, 52, 1997
6 Serizawa A, Hirosawa S, Sato T, Metall Mater Trans A 2008, 3: 243-251
7 M.J. Starink, N. Gao, L. Davin, J. Yan, A. Cerezo. Phil. Mag. 2005, 85: 1395
8 N. Kamp, N. Gao, M.J. Starink, I. Sinclair. Int. J. Fatigue 2007, 29: 869-878
9 J.C. Williams, E.A. Starke, Acta Mater 2003, 51: 5775-5799
10 Bastow TJ, Phil.Mag. 2005, 85: 1053
11 Bastow TJ, Hill AJ. Mater. Sci. For. 519-521: 1355-1360, 2006.
12 T.E.M. Staab, M. Haaks, H. Modrow. Appl Surf Sci 2008, 255, 132-135.
13 B. Klobes, T.E.M. Staab, M. Haaks, K. Maier and I Wieler. Phys Stat Sol 2008, 2, A61 - A66.
14 H.K. Hardy, J. Inst. Metals 1954-55, 83: 17.
15 J.T. Vietz, I.J. Polmear. J. Inst. Metals 1966, 94: 410.
16 T. Takahashi, T. Sato. J. Jpn. Inst. Light Metals 1985, 35, 41.
17 Y. Nagai, M. Murayama, Z. Tang, T. Nonaka, K. Hono and M. Hasegawa, Acta Mater. 49 (2001) 913.

18 S. Abis, M. Massazza, P. Mengucci, G. Riontino. Scr. Mater. 2001,45: 685 .
19 M.J. Starink, A. Cerezo, J. Yan, N. Gao. Philosoph. Mag Lett 2006, 86:243
20 S.P. Ringer, T. Sakurai, I.J. Polmear. Acta Mater. 1997, 45: 3731.
21 S.P. Ringer, S.K. Caraher, I.J. Polmear. Scr. Mater. 1998, 39: 1559.
22 A.-M. Zahra, C.Y. Zahra. Phil. Mag. Lett. 2002, 82: 9
23 L. Kovarik, S.A. Court, H.L. Fraser, M.J. Mills. Acta Mater 2008, 56: 4804-4815
24 Aiwu Zhu, B.M. Gable, G.J. Shiflet, E.A. Starke. Acta Mater. 2004, 52: 3671
25 Aiwu Zhu, Jr., E.A. Starke and G.J. Shiflet. Scripta Mater. 2005, 53: 35
26 S.C. Wang, M.J. Starink. Int Mater Rev., 2005, 50:193
27 F. Bron, J. Besson, A. Pineau. Mater. Sci. Eng. A 2004, 380;356.
28 A.J. Ardell. Metall. Trans. A. 1985, 16: 2131.
29 C. Schlieser and E. Nembach. Acta Metall. Mater. 1995, 43:3983.
30 V. Gerold, H.J. Gudladt and J. Lendvai. Phys Stat Sol A 1992, 131:509
31 E. Nembach. Scr. Mater 1997, 36:1409.
32 S.M. Jeon, J.K. Park, Acta Mater. 1996, 4: 1449
33 A.R. Büchner. W. Pitsch. Z. Metallkde 1985, 76: 651.
34 P.A. Flinn. Acta Metall 1958, 6: 631
35 G. Kostorz. B. Schonfeld. Chimia 2001,55:517
36 T. Mohri, H. Miyamoto, Y. Terada,d T. Suzuki. Mater Sci Eng A 1999, 267:151
37 L. Cartaud, J. Guillot and J. Grilhe. Proc of ICSMA IV, Nancy, 30 August–3 September 1976, vol. 1, (Ed. Laboratoire de Physique du Solide ENSMIN-INPL, Nancy) p. 214 (1976).
38 P. Gomiero, Y. Brechet, F. Louchet, A. Tourabi, B. Wack. Acta Metall. Mater. 1992, 40:857.
39 C.J. Smithells, Metals Reference Book, 7th Ed., Butterworths-Heinemann, London, 1992.
40 E. Nembach. Phys. Stat. Sol. A, 1983, 78, 571
41 S.C. Wang, Z. Zhu. M.J. Starink, J. Microscopy, 2005, 217: 174.
42 Z. Zhu, M.J. Starink. Mater Sci Eng A, 2008, 488: 125
43 M.J. Starink, Int. Mater. Rev. 2004, 49: 191
44 M.J. Starink and A. Dion, Thermochim Acta 2004, 417:5
45 J. Yan, PhD thesis, University of Southampton, 2006
46 L. Kovarik, P.I. Gouma, C. Kisielowski, S.A. Court, M.J. Mills. Mater. Sci. Eng. 2004 A387-389: 326
47 L. Kovarik, P.I. Gouma, C. Kisielowski, S.A. Court and M.J. Mills, Acta Mater. 2004, 52:2509
48 M.J. Starink. Thermochim. Acta, 2003, 404:163
49 I.N. Khan and M.J. Starink. Mater. Sci. Techn., 2008, 24: 1403-1410
50 M.J. Starink and P.J. Gregson. Scr. Metall. Mater. 1995, 33: 893
51 L. Davin. PhD thesis, Oxford University, 2004
52 A.-M. Zahra, C. Zahra and B. Verlinden. Phil Mag Lett. 2006, 86:235
53 B. Verlinden, A.-M. Zahra. Mater. Sci. Forum 2003, 426-432: 423
54 Charai, A., Walther, T., Alfonso, C., Zahra, A. M., Zahra, C. Y.: Acta Mater. 2000, 48:2751
55 M.J. Starink, A. Deschamps, S.C. Wang. Scr Mater, 2008, 58: 377
56 I.N. Khan, M.J. Starink, J.L. Yan. Mater. Sci. Eng. A, 2008,472:66
57 Z. Zhu, M.J. Starink. Mater. Sci. Eng. A 2008, 489:138
58 Weilong Hu. Int. J. Plast. 2007, 23:620
59 R.N. Wilson, D.M. Moore, P.J.E. Forsyth. J Inst Met 1967, 95: 177
60 I.J. Polmear, Trans Met Soc AIME 1964, 230: 1331
61 K. Raviprasad, ICAA9, 2-5 August 2004, Brisbane, Australia (poster)
62 G.B. Winkelman, K. Raviprasad, B.C. Muddle. Mater Sci Forum 2002, 396:1037
63 J.R. Davis (ed.), ASM Specialty Handbook Aluminum and Aluminum Alloys (ASM International) 1993
64 T.S. Srivatsan, D. Kolar and P. Magnusen. Materials & Design 2002, 23:129.
65 P. Ratchev, B. Verlinden, P. De Smet and P. Van Houtte, Acta Mater. 1998, 46:3523.
66 S.A. Court, L. Kovarik and M.J. Mills. unpublished research, 2006
67 W.L. Fink, D.W. Smith, L.A. Willey. in 'Age Hardening of Metals', Symposium on Precipitation Hardening, Chicago, Oct 23-27, 1939, American Society for Metals (1940).
68 L. Reich, S.P. Ringer and K. Hono. Phil. Mag. Lett. 1999, 79:639.
69 S. Katsikis, B. Noble, S.J. Harris. Mater Sci Eng 2008, A485; 613.
70 P. Villars, A. Prince, H. Okamoto (Eds.). Handbook of ternary alloy phase diagrams, ASM International, Materials Park, OH, 1994.
71 H.W.L. Phillips. 'The constitution of alloys of aluminium, copper and iron', J. Inst. Met., 1953-54, 82: 197.